Quantification of Gd-BOPTA uptake and biliary excretion from dynamic magnetic resonance imaging in rat livers: model validation with 153Gd-BOPTA

Planchamp, Corinne; Pastor, Catherine; Balant, Luc; Becker, Christoph; Terrier, François; Gex-Fabry, Marianne

How to cite

PLANCHAMP, Corinne et al. Quantification of Gd-BOPTA uptake and biliary excretion from dynamic magnetic resonance imaging in rat livers: model validation with 153Gd-BOPTA. In: Investigative radiology, 2005, vol. 40, n° 11, p. 705–714. doi: 10.1097/01.rli.0000183053.08921.2b

This publication URL: https://archive-ouverte.unige.ch/unige:40291
Publication DOI: 10.1097/01.rli.0000183053.08921.2b

Quantification of Gd-BOPTA Uptake and Biliary Excretion From Dynamic Magnetic Resonance Imaging in Rat Livers

Model Validation With ^{153}Gd-BOPTA

Corinne Planchamp, PhD, Catherine M. Pastor, MD, PhD,* Luc Balant, PhD,† Christoph D. Becker, MD,* François Terrier, MD,* and Marianne Gex-Fabry, PhD†*

Objectives: We sought to develop and validate a pharmacokinetic model allowing description of the magnetic resonance (MR) signal intensity induced by the hepatobiliary contrast agent Gd-BOPTA and to quantify the overall Gd-BOPTA transport in rat liver.

Materials and Methods: MR signal intensity was recorded during the perfusion of rat livers with Gd-DTPA, an extracellular contrast agent, and Gd-BOPTA, a hepatobiliary contrast agent. Similar experiments were conducted with ^{153}Gd-labeled contrast agents for quantitative measurement in liver, bile and perfusate.

Results: A complete 6-compartment, 8 parameter open model was first developed to describe the pharmacokinetics of the compound based on the radioactivity data analysis. Because perfusate and bile data were not available in MRI experiments, a reduced model (6-compartment, 5 parameters) was considered for the MRI data. The performance of the reduced model was tested using the radioactivity data. The reduced model successfully described the contrast agent amount in the liver and correctly predicted amounts in bile and perfusate.

Conclusions: Pharmacokinetic modeling of MR signal intensity induced by Gd-BOPTA permits quantification of Gd-BOPTA uptake and biliary excretion in rat livers.

Key Words: MRI, contrast agent, liver, Gd-BOPTA, pharmacokinetic model

(*Invest Radiol* 2005;40: 705–714)

Gadobenate dimeglumine (Gd-BOPTA/Dimeg, MultiHance, Bracco Imaging, Italy) is a newly commercialized magnetic resonance imaging (MRI) contrast agent that combines the properties of a conventional extracellular contrast agent such as gadopentetate dimeglumine (Gd-DTPA/Dimeg, Magnevist, Schering, Germany) with those of a hepatobiliary contrast agent that enters into hepatocytes with subsequent biliary excretion. This feature enables Gd-BOPTA/Dimeg to be used similarly to Gd-DTPA/Dimeg to detect hypervascular regions in the postinjection phase and to improve the detection and characterization of hepatic diseases in the delayed hepatobiliary phase.[1–4]

Gadobenate ion (Gd-BOPTA), the moiety of gadobenate dimeglumine responsible for the signal enhancement, is partially taken up into hepatocytes and excreted without biotransformation.[5,6] In rats, approximately 50% of the injected dose (0.1 to 0.5 mmol/kg) is excreted into bile, with the remaining fraction being excreted into urine.[6] In contrast, only 2–4% of the dose (0.005 to 0.2 mmol/kg) is excreted into bile in humans.[7] Experimental evidences exist that Gd-BOPTA enters into rat hepatocytes through a transporter belonging to the organic anion transporting polypeptide family (Oatps) localized on the sinusoidal membrane of hepatocytes.[8–10] After its intracellular transport, Gd-BOPTA is eliminated into bile through the ATP-dependent multidrug resistance-associated protein 2 (Mrp2) at the canalicular membrane of hepatocytes.[11,12]

Compartmental pharmacokinetic analysis of MRI data obtained after injection of extracellular contrast agents has previously been developed to measure the perfusion of organs such as heart[13,14] and liver,[15–18] and to assess the permeability of tissues such as blood-brain barrier.[19–21] Contrast-enhanced MRI pharmacokinetic analysis has emerged as a promising technique in oncology for tumor staging, response to treatment, and development of effective antitumoral drugs.[22–24] In these analyses, compartmental models assess the distribution of extracellular contrast agents between blood and interstitial space.[25,26] To our knowledge, no compartmental pharmacokinetic analysis of MR signal intensity has yet been reported when MRI is performed with hepatobiliary contrast agents that enter into hepatocytes and are eliminated by the bile.

In the isolated perfused rat liver, we previously demonstrated that the increase in MR signal intensity during Gd-BOPTA perfusion could be recorded over time, with direct visualization of the absence of Gd-BOPTA entry into

Received June 3, 2005 and accepted for publication, after revision, July 21, 2005.

From the *Department of Radiology and †Department of Psychiatry, Geneva University Hospitals, Geneva, Switzerland.

Supported by the "Fonds National Suisse de la Recherche Scientifique" no 3200-100 868 to C. M. Pastor.

Reprints: Corinne Planchamp, PhD, Hôpitaux Universitaires de Genève, Laboratoire de physiopathologie hépatique et imagerie moléculaire, Département de Radiologie, Rue Micheli-du-Crest 24, CH-1211 Genève 14. E-mail: corinne.planchamp@hcuge.ch.

ISSN: 0020-9996/05/4011-0705

hepatocytes when livers were coperfused with bromosulfophthalein (pharmacological inhibition).[10] We also showed that Gd-BOPTA-induced signal intensity enhancement remained similar in mild cirrhotic and normal rats but significantly decreased in severe cirrhosis.[27] Moreover, in a hollow-fiber bioreactor containing freshly isolated rat hepatocytes, we showed that the transport of Gd-BOPTA into hepatocytes can be successfully described by compartmental pharmacokinetic analysis of the MR signal intensity, supporting the hypothesis of a transporter-mediated uptake.[28] The aim of the present study was to extend such a pharmacokinetic model to describe the overall Gd-BOPTA transport in perfused in situ rat livers by recording MR signal intensity over time. The modeling process integrated information from both extracellular Gd-DTPA and hepatobiliary Gd-BOPTA. Since MR signal intensity did not provide direct quantification of hepatic amount of contrast agent, model development considered additional data obtained from ^{153}Gd-labeled Gd-DTPA and Gd-BOPTA that assessed the exact amounts of contrast agents in liver as well as in bile and perfusate.

MATERIALS AND METHODS

Chemicals

Gd-BOPTA/Dimeg and Gd-DTPA/Dimeg are commercially available. $^{153}GdCl_3$ (1 GBq/mL) was obtained from Gamma-Service Isotopen und Strahlentechnik GmbH (Leipzig, Germany). All other chemicals were of analytical grade. ^{153}Gd-labeled Gd-DTPA and Gd-BOPTA were obtained by adding $^{153}GdCl_3$ to the commercially available 0.5 M solutions (1 MBq/mL) that contain a slight excess of ligand DTPA and BOPTA. Contrast agents were diluted in Krebs-Henseleit-bicarbonate (KHB) solution to obtain a 500 μM concentration in the perfusion solution.

Animals

Before liver perfusion, 7 Sprague-Dawley rats (Charles River, l'Arbreste, France, 300–450 g) were anesthetized with pentobarbital (50 mg/kg ip). The protocol was approved by the animal welfare committee of the University of Geneva and the veterinary office and followed the guidelines for the care and use of laboratory animals.

Liver Perfusion

Livers were perfused in situ as previously described.[29] Briefly, the abdominal cavity was opened and the portal vein was cannulated with a G16 catheter (outer diameter: 1.8 mm) introduced into the portal vein up to 2–3 mm from the liver. A ligature was placed around the inferior vena cava above the left renal vein. After cannulation of the portal vein, the abdominal vena cava was transected and KHB solution was pumped without delay into the portal vein. The flow rate was slowly increased over the course of 1 minute up to 30 mL/min. In a second step, the chest was opened and a second cannula (G14) inserted through the right atrium into the thoracic inferior vena cava and secured with a ligature. Finally, the ligature around the abdominal inferior vena cava was tightened. The KHB solution was perfused to the liver through the portal catheter and eliminated by the catheter placed in the thoracic inferior vena cava. When livers were perfused with ^{153}Gd-labeled contrast agents, the common bile duct was cannulated with a PE 10 catheter.

To evidence the extracellular diffusion space, each liver was perfused with KHB solution + Gd-DTPA (30 minutes), followed by KHB solution for washing (15 minutes). To study the hepatocyte entry of Gd-BOPTA, the same liver was perfused with KHB solution + Gd-BOPTA (30 minutes), followed by KHB solution for washing (30 minutes). In each liver, Gd-DTPA was perfused before Gd-BOPTA. Because a steady-state was rapidly reached with Gd-DTPA and to limit the use of radioactivity, Gd-DTPA was only perfused during 15 minutes in the radioactivity experiments. During perfusion, the liver viability was assessed by monitoring portal vein pressure (Hewlett Packard 78353B, Palo Alto, CA). Under these conditions, the perfusion of both contrast agents modified neither the hepatic O_2 consumption nor the portal pressure.[10]

The entire perfusion system consisted of reservoir for perfusion solution, pump, heating circulator, oxygenator, filter, bubble trap, temperature probe and perfusate collector. The livers were perfused with a nonrecirculating solution during the entire protocol. The perfusate was equilibrated in the oxygenator with a mixture of 95% O_2–5% CO_2 (2.5 L/min). The temperature was measured continuously with a thermocouple thermometer (Extech Instruments Co, no 422315, Waltham, MA), the temperature probe being placed upstream from the portal vein catheter.

Radioactivity Experiments

A gamma scintillation probe with a sodium chloride crystal (thickness 2.5 cm, diameter 2.5 cm, Canberra Eurisys, France) and a lead collimator (thickness 1 cm, opening diameter 0.8 cm) were placed 1 cm over the liver (n = 3). Counts were summarized every 20 seconds with a multichannel analyzer. Homogenous uptake of the radioactivity into the liver was checked in preliminary studies: similar results were obtained when the probe was positioned at various locations over the liver. Bile and outflow perfusate samples were collected every 5 minutes, weighted and the radioactivity was determined by a Packard Cobra Auto-Gamma counter (Canberra Packard, Schlieren, Switzerland). At the end of each experiment, portal vein, thoracic inferior vena cava and bile duct were clamped and the liver was removed and weighted. To translate probe counts into contrast agent amounts, the total radioactivity in the whole liver was measured with a dose calibrator (Isomed 2000, MED Nuklear-Medizintechnik, Dresden, Germany) and related to the last count measured by the probe. In each experiment, the amount of contrast agent perfused was totally recovered in perfusate, liver, and bile and confirmed that each experiment was correctly conducted.

MRI Experiments

Livers in the carcass were inserted into a wrist coil (n = 4). Because of MR incompatibility, all material containing metal (heating circulator, O_2-CO_2 tank and the pump) was installed in an adjacent room. MRI was performed on a 1.5-T Eclipse MR system (Philips Medical System, Cleveland, OH). An axial image was obtained using a fast-gradient

echo T1 weighted MR sequence (FAST) preceded by a 90° saturation pulse with the following parameters: inversion time (29 milliseconds); repetition time (6.8 milliseconds); echo time (3 milliseconds); flip angle (90°); matrix 256 × 256; 1 image/8 seconds; FOV 14 cm; slice thickness 7 mm. Mean signal intensity was measured in a region of interest drawn on the short axis view of the liver to encompass a hepatic lobe. The signal intensity measured in the liver was normalized to muscle signal intensity. For each liver, the region of interest remained constant during the entire experiment, but could vary between livers.

Pharmacokinetic Model, Implementation, and Evaluation

We previously showed that a 2-compartment model adequately described signal intensity-time curves obtained during Gd-DTPA and Gd-BOPTA perfusion in a hollow-fiber bioreactor containing isolated hepatocytes.[28] In the present study, a compartmental modeling approach was employed to describe the kinetics of ^{153}Gd-labeled Gd-DTPA and Gd-BOPTA in the isolated perfused livers, amounts of contrast agent being also measured in perfusate and bile. Consequently, a model with 4 compartments was used as a starting point (Fig. 1, compartments 1 to 4). Compartments 1 and 2 described the liver: compartment 1 depicted the amount of contrast agent in extracellular space $A_1(t)$ and compartment 2 the amount in hepatocytes $A_2(t)$. Compartment 3 represented the amount of contrast agent in the outflow perfusate $A_3(t)$ and compartment 4 the amount of contrast agent in bile $A_4(t)$. Extension of the model was necessary to successfully describe data in the isolated perfused liver. It proceeded in 2 steps: compartment 5, with amount of contrast agent $A_5(t)$, reflected the in-homogeneity of the perfusion solution at the beginning and end of perfusion of contrast agent (mixing of KHB with contrast agent solution in the perfusion system), and compartment 6 depicted amount of contrast agent in a secondary hepatocyte-associated space $A_6(t)$. Entry of contrast agent into the system was modeled as a zero-order infusion rate K_{in} over a time period τ. First-order rate constants k_{ij} were defined with respect to the compartment of origin i and the compartment of convergence j. The amount versus time profiles of both Gd-DTPA and Gd-BOPTA were simultaneously modeled. Because they shared the same access to the system and extracellular space, k_{51} and k_{13} were considered identical. The possibility that Gd-DTPA entered into the cellular compartment 2 with a rate constant k_{12} that differed from Gd-BOPTA was considered.

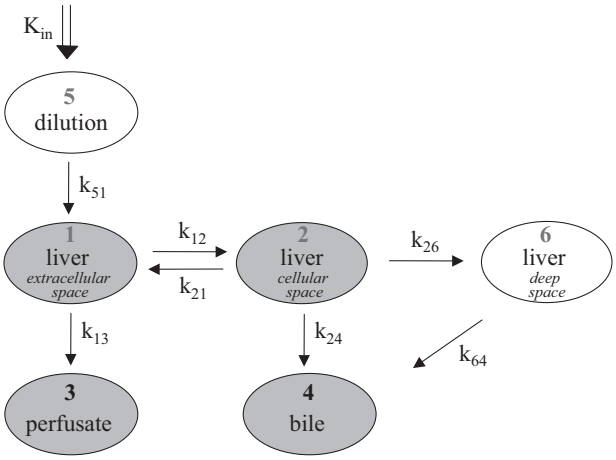

FIGURE 1. Pharmacokinetic model. Entry of contrast agents into the perfused rat liver was modeled as a zero-order infusion rate K_{in}. A model with 4 compartments was first considered (gray compartments). Compartments 1 and 2 described the liver: compartment 1 depicted the amount of contrast agent in extracellular space and compartment 2 the amount in hepatocytes. Compartment 3 represented the amount of contrast agent in the outflow perfusate and compartment 4 the amount of contrast agent in bile. Extension of the model was necessary to successfully describe the data: compartment 5 illustrated the in-homogeneity of the perfusion solution at the beginning and end of perfusion of contrast agents, and compartment 6 depicted the trapping of contrast agent in a secondary hepatocyte-associated space. First-order rate constants k_{ij} are defined with respect to compartment of origin i and compartment of convergence j.

This complete 6-compartment model was first developed for radioactivity data. Because perfusate and bile data were not available in the MRI experiments, the complete model had too many parameters to be fully reconciled with MRI data of the liver and a reduced 6-compartment model was thus used. To validate the reduced model used for the MRI data, the reduced model was applied to the radioactivity data of the perfused liver ignoring bile and perfusate data. Validation through parameters proceeded by comparison of estimates from the reduced and complete models. Validation through predictions considered predicted amounts of contrast agent in bile and perfusate with respect to experimental data from radioactivity experiments. Mean prediction error was calculated from the differences between observed and predicted amounts.

The model was implemented in the NONMEM software (version V, University of California, San Francisco, CA). Originally developed for population pharmacokinetics, ie, analysis of interindividual variability on the basis of sparse data in large patient populations, NONMEM offers a flexible programming environment. In particular, it can integrate data obtained from different substances (Gd-DTPA and Gd-BOPTA) in different samples (liver, perfusate and bile) with specific error models. Subroutines ADVAN6 and TRANS1 were used for model description.

Parameter estimation proceeded by minimizing an objective function that is a statistical measure of the overall distance between the model and the data. To identify the best model during the development phase, statistical comparison of models was based on a likelihood ratio test, ie, a χ^2 test of the difference of objective functions (the lower the value, the better the fit), with $P < 0.01$ considered to represent a significantly better fit (ie, $\chi^2 > 6.6$). In addition, standard errors of parameter estimates and correlations between them were considered. Graphical assessment of the goodness of fit was performed through analysis of residuals (ie, differences between measured and predicted amounts). The absence of bias was also checked (no significant bias if the 95% confi-

dence interval of the residuals comprised 0). When 2 models performed similarly, the simplest model was selected (principle of parsimony).

Modeling Radioactivity Data

Observed amounts in perfusate, bile and liver were modeled as follows:

$$A_{perfusate}(t)_{obs} = A_3(t)_{pred} \cdot (1 + \epsilon_1) \quad (1)$$

$$A_{bile}(t)_{obs} = A_4(t)_{pred} \cdot (1 + \epsilon_2) \quad (2)$$

$$A_{liver}(t)_{obs} = A_1(t)_{pred} + A_2(t)_{pred} + A_6(t)_{pred} + \epsilon_3 + \sqrt{A_1(t)_{pred} + A_2(t)_{pred} + A_6(t)_{pred}} \cdot \epsilon_4 \quad (3)$$

where ϵ_1, ϵ_2, ϵ_3, and ϵ_4 are random residual errors assumed to be normally distributed with mean 0 and corresponding variances σ_1^2, σ_2^2, σ_3^2, and σ_4^2. Various models of errors were applied and the most suitable in terms of objective function and residuals were chosen. For cumulative amounts in perfusate and bile, proportional errors were selected (ϵ_1 and ϵ_2 in eq 1 and 2). For amount in the liver, a mixed error model was considered that included both an additive term (ϵ_3 in eq 3) and a term taking into account that error of radioactivity measurements is proportional to the square root of counts (ϵ_4 in eq 3). In addition to the rate constants describing the model, error variances σ_1^2, σ_2^2, σ_3^2, and σ_4^2 were estimated.

Modeling MRI Data

Because the signal intensity and not the amount of contrast agent was analyzed with MRI data, the relationship between signal intensity and amount of contrast agent was considered. Similarly to the equation developed for the hollow fiber bioreactor containing rat hepatocytes,[28] the average signal intensity (indicated as SI) in the region of interest in the liver was:

$$SI(t)_{pred} = s_0 + g_1 \cdot A_1(t) + g_2 \cdot A_2(t) + g_6 \cdot A_6(t) \quad (4)$$

where s_0 is baseline signal, g_1, g_2, and g_6 are tissue-specific constants of proportionality depending on native relaxation rate and relaxivity.[30] As a first approximation, a single proportionality constant ($g = g_1 = g_2 = g_6$) was assumed and equation 4 was rewritten as:

$$SI(t)_{pred} = s_0 + g[A_1(t) + A_2(t) + A_6(t)] \quad (5)$$

To include the possibility of signal saturation, an alternative hyperbolic signal intensity model was considered:

$$SI(t)_{pred} = s_0 + g\frac{[A_1(t) + A_2(t) + A_6(t)] \cdot ASAT_{50}}{[A_1(t) + A_2(t) + A_6(t)] + ASAT_{50}} \quad (6)$$

where $ASAT_{50}$ is the amount of contrast agent leading to half maximum signal enhancement.

Observed signal intensity $SI(t)_{obs}$ was modeled as:

$$SI(t)_{obs} = SI(t)_{pred} \cdot (1 + \epsilon) \quad (7)$$

where $SI(t)_{pred}$ is the predicted signal intensity according to equation 5 or 6 and ϵ is a proportional error assumed to be normally distributed with mean 0 and variance σ^2. In addition to rate constants, the saturation parameter $ASAT_{50}$, the proportionality constant g and error variance σ^2 were estimated. S_0 was a fixed parameter determined prior to modeling for each experiment, considering the mean signal intensity preceding the start of perfusion.

RESULTS

Radioactivity Data

During the perfusion of 500 μM Gd-DTPA (450 mL, 225 μmoles) the hepatic amount of contrast agent rapidly increased toward steady-state (1.5–1.7 μmoles) and Gd-DTPA was completely washed out during the subsequent KHB perfusion (Fig. 2). No Gd-DTPA was excreted into bile, no Gd-DTPA remained in the liver, and 225 μmoles (100% of the perfused dose) were recovered in the perfusate after perfusion and washing. During the perfusion of 500 μM Gd-BOPTA (900 mL, 450 μmoles), the contrast agent amount in the liver increased as much as 10–12 μmoles. After perfusion and washing of Gd-BOPTA, 1.7–2.8 μmoles (0.5% of the perfused dose) remained in the liver, 18–22 μmoles were excreted into bile (4.5% of the perfused dose), and 426–428 μmoles (95% of the perfused dose) were recovered in the perfusate.

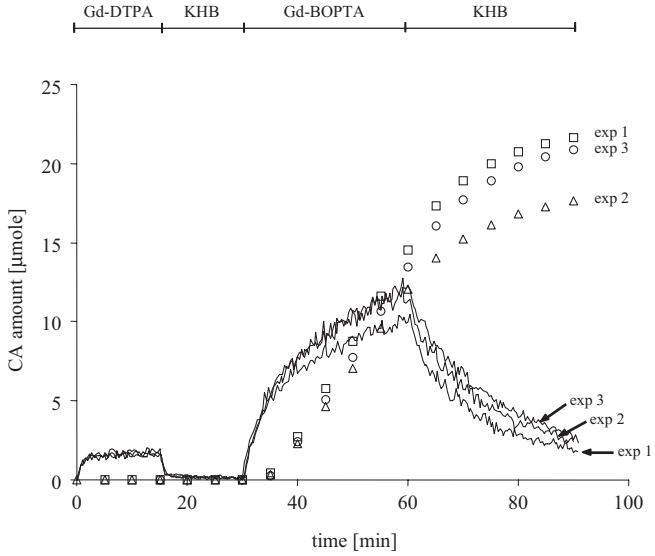

FIGURE 2. Radioactivity detection: amount of contrast agent in liver and bile during the perfusion of 500 μM Gd-DTPA (15 minutes, 450 mL, 225 μmoles), KHB solution (15 minutes), 500 μM Gd-BOPTA (30 minutes, 900 mL, 450 μmoles), and KHB (30 minutes). Liver, continuous line; bile, symbols. Exp 1, exp 2, and exp 3 refer to 3 different liver perfusions.

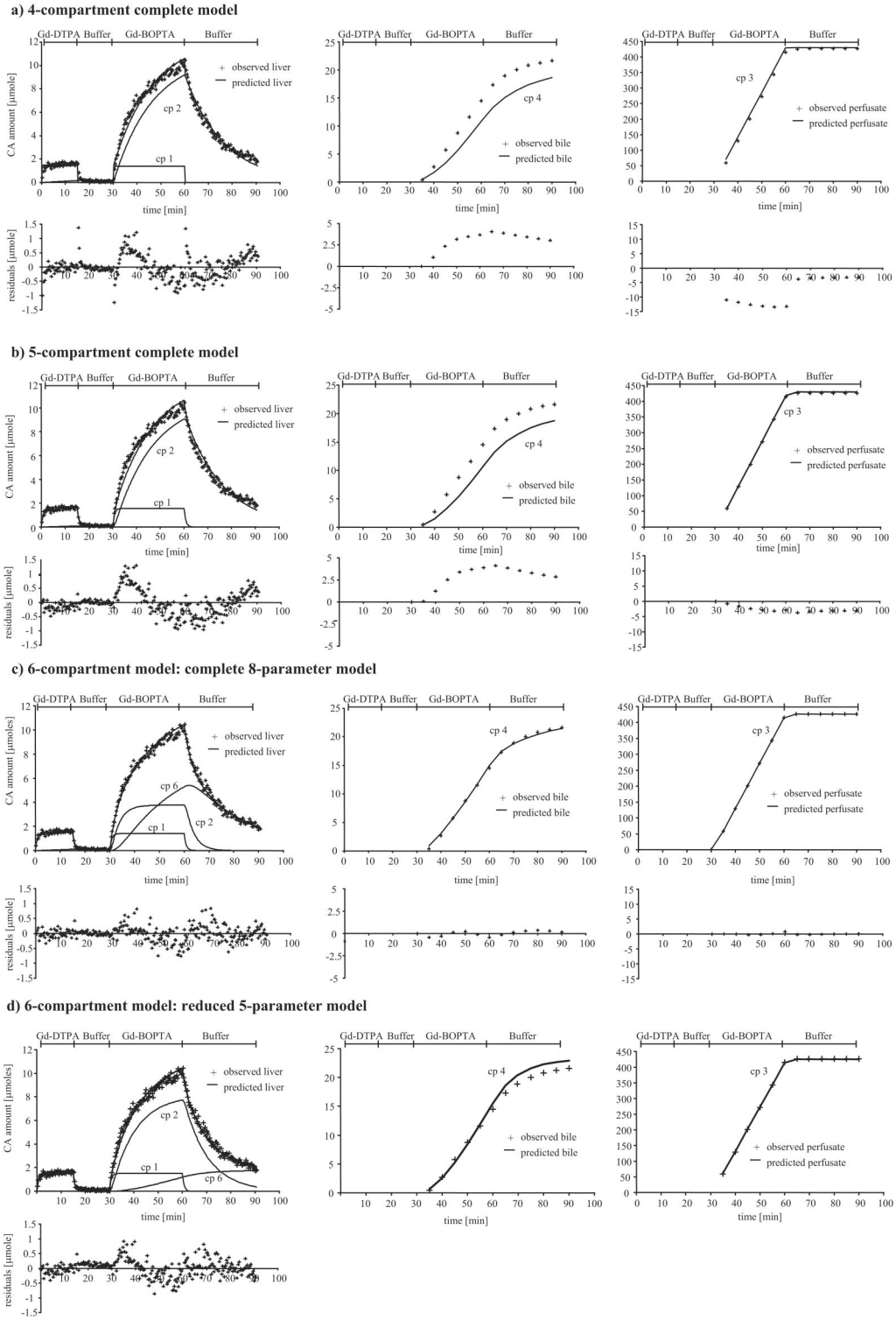

FIGURE 3. Radioactivity detection: observed and model-predicted amount of contrast agent in liver, bile and perfusate during the perfusion of Gd-BOPTA, Gd-DTPA acting as an indicator of the extracellular distribution. a, Predictions from the 4-compartment complete model. b, Predictions from the 5-compartment complete model. c, Predictions from the complete 6-compartment 8-parameter model. d, Predictions from the reduced 6-compartment 5-parameter model on the basis of liver data only. For clarity, the result of a single experiment (exp 1) is shown but all other experiments performed similarly. cp, compartment.

Compartmental analysis of the data was first performed with a 4-compartment model (Fig. 3a) to represent extracellular volume of the liver (compartment 1), intracellular volume of the liver (compartment 2), perfusate (compartment 3), and bile (compartment 4). This model did not successfully describe the data (objective function: −134). Predicted increase and decrease of contrast agent amounts into compartment 1 was too rapid to describe the amounts observed, as reflected by large residuals at 0, 15, 30, and 60 minutes. Moreover, the amount of Gd-BOPTA in bile and perfusate were respectively under- and over-estimated. The fits were improved by addition of a compartment (Fig. 3b) that depicted the in-homogeneity of the perfusion solution at the beginning and end of perfusion of contrast agent (compartment 5). With this additional compartment, the range of residuals in the liver and perfusate decreased as well as the objective function (–268). Nevertheless, the fits of the amounts of Gd-BOPTA in liver, bile and perfusate were still unsatisfactory. The addition of a secondary cellular compartment (compartment 6) with access to bile improved the fits of liver, bile and perfusate. The range of residuals decreased, their distribution was homogenous and the objective function diminished (−616; Fig. 3c).

Estimated rate constants are summarized in Table 1. For Gd-DTPA, the best fit was obtained with a minor unidirectional exchange with the cellular compartment 2 (k_{12}(D)). This model was significantly better than without access to compartment 2 (likelihood ratio test of objective functions, $P < 0.01$). In contrast, Gd-BOPTA had a much higher distribution to cellular compartments with k_{12}(B) more than 100 times higher than k_{12}(D). Hence, a 6-compartment model with 8 rate constants was the simplest model that successfully described the experimental data.

The precision of all estimates was adequate, with standard errors <10% in the 3 experiments except for k_{21}(B) (standard errors <25%) and k_{26}(B) (standard errors <15%). Between-experiment variability was low for all parameters except for k_{21}(B) that displayed 3-fold variability. Coefficients of variation of the residual error were <0.2% and 15% for perfusate and bile, respectively, for the 3 experiments. Taking into account the mixed error in the liver (eq 3), standard deviations of the residual error were <0.1 μmoles and <0.5 μmoles when amounts in the liver were 0 and 11 μmoles, respectively.

As illustrated in Figure 3c, predictions in extracellular compartment 1 were similar for Gd-DTPA and Gd-BOPTA as postulated in the model. Steady-state was rapidly reached and contrast agents were totally eliminated during washing. Amount of Gd-BOPTA in cellular compartment 2 reached steady-state more slowly than in compartment 1 and was completely eliminated during washing. In contrast, the amount in cellular compartment 6 continuously increased during Gd-BOPTA perfusion and slowly decreased during washing, without returning to baseline level over the 90-minute observation period.

MRI Data

During Gd-DTPA perfusion, signal intensity in the liver increased toward steady-state (0.3–0.8 over baseline) and rapidly returned to baseline value during the washout period (Fig. 4). The signal intensity was much higher when livers were perfused with Gd-BOPTA (1.7–3.3). In contrast to Gd-DTPA perfusion, the signal intensity did not return to baseline value during the washout period.

The complete 6-compartment model with 8 rate constants developed for the radioactivity data was not compatible

TABLE 1. Rate Constants Estimated From Fitting Radioactivity and MRI Data With the 6-Compartment Model

	k_{51} (D and B) (min^{-1})	k_{13} (D and B) (min^{-1})	k_{12}(D) (min^{-1})	k_{12}(B) (min^{-1})	k_{21}(B) (min^{-1})	k_{26}(B) (min^{-1})	k_{24}(B) (min^{-1})	k_{64}(B) (min^{-1})	$ASAT_{50}$ (μmoles)
Radioactivity data									
Complete model									
Exp 1	1.5	10.0	0.005	0.8	0.11	0.09	0.12	0.043	—
Exp 2	1.7	9.3	0.009	1.1	0.28	0.14	0.07	0.043	—
Exp 3	1.8	10.1	0.006	0.8	0.09	0.12	0.09	0.040	—
Mean ± SD	1.7 ± 0.2	9.8 ± 0.4	0.007 ± 0.002	0.9 ± 0.1	0.16 ± 0.10	0.11 ± 0.02	0.09 ± 0.02	0.042 ± 0.001	—
Reduced model									
Exp 1	1.6	9.4	—	0.55	—	0.007	0.09	—	—
Exp 2	2.4	8.5	—	0.54	—	0.008	0.09	—	—
Exp 3	1.6	9.3	—	0.57	—	0.007	0.07	—	—
Mean ± SD	1.8 ± 0.4	9.1 ± 0.5	—	0.55 ± 0.01	—	0.007 ± 0.001	0.08 ± 0.01	—	—
MRI data									
Reduced model									
Exp 4	1.1	10.0	—	0.4	—	0.007	0.08	—	11
Exp 5	0.7	9.6	—	0.5	—	0.002	0.05	—	9
Exp 6	2.5	10.9	—	2.5	—	0.002	0.10	—	17
Exp 7	1.3	10.6	—	0.9	—	0.003	0.08	—	14
Mean ± SD	1.4 ± 0.7	10.3 ± 0.6	—	1.1 ± 1.0	—	0.004 ± 0.002	0.08 ± 0.02	—	13 ± 3

D refers to Gd-DTPA and B to Gd-BOPTA. Gd-DTPA and Gd-BOPTA shared the same access to the system and extracellular space; therefore, k_{51} and k_{13} were considered identical. Gd-DTPA was allowed to enter into the cellular compartment 2 with a rate constant k_{12} that differed from Gd-BOPTA.

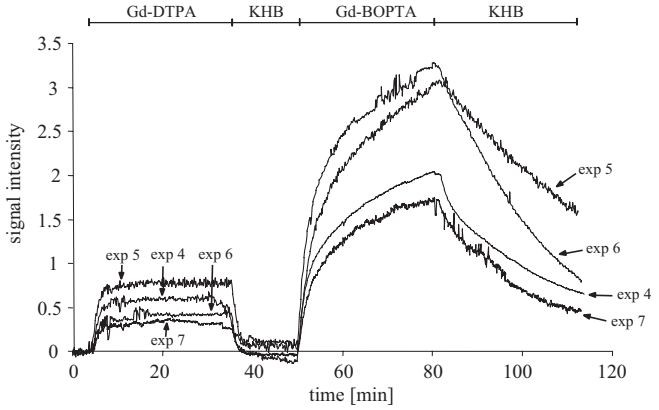

FIGURE 4. MR signal intensity (arbitrary unit) in liver during the perfusion of 500 μM Gd-DTPA (30 minutes), KHB solution (15 minutes), 500 μM Gd-BOPTA (30 minutes), and KHB (30 minutes). Experiments in 4 different livers are illustrated (exp 4 to exp 7). Background signal was subtracted from the data.

with MRI data, as expected from the absence of perfusate and bile data in these experiments. k_{51}(D and B), k_{13}(D and B), k_{12}(B), k_{24}(B), and k_{26}(B) were fully identifiable contrary to k_{21}(B), k_{64}(B) and k_{12}(D) which were thus set to 0 (Table 1). It was not possible to determine the proportionality constant g relating signal intensity to amount from MRI data. Thus, g was calculated a priori for each experiment according to equation 5, considering signal intensity over baseline at Gd-DTPA steady-state, amount in extracellular liver volume being estimated from average extracellular volume (25% of total liver volume, ie, 3 mL) and concentration perfused (500 μM).

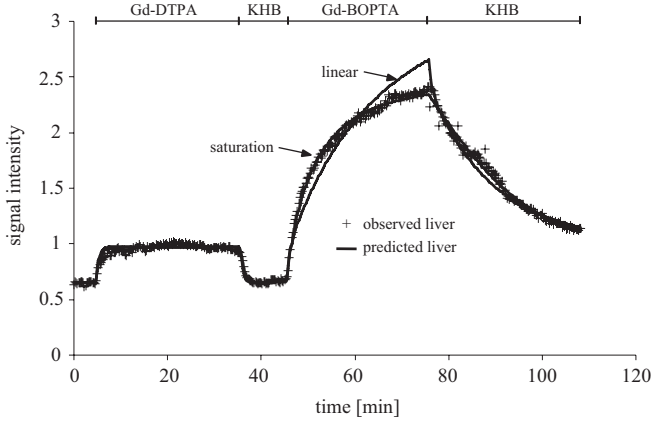

FIGURE 5. Observed and model-predicted MR signal intensity (arbitrary unit) in liver during the perfusion of Gd-DTPA and Gd-BOPTA. Model that included a saturation term in the equation relating signal intensity to amount of contrast agent (eq 6) adequately fitted the experimental data, in contrast to the same model that considered a linear relationship between signal intensity and amount of contrast agent (eq 5). For clarity, the result of a single experiment (exp 7) is shown but the other experiments performed similarly.

As seen in Figure 5, the data were successfully described when signal saturation was considered (eq 6) but not when considering a linear relationship between signal intensity and amount of contrast agent (eq 5). The precision of the parameter estimates was adequate, with standard errors $<$10% for all parameters in the 4 experiments. Between-experiment variability was large for all parameters except for k_{13}(D and B). Residual error on signal intensity was $<$4%.

The reduced model estimated similar rate constants from MRI data than the complete model from radioactivity data, except for k_{26}(B) that was about 25 times lower in the MRI experiments. The model predicted Gd-BOPTA amounts in bile (18–40 μmoles) close to those obtained with radioactivity experiments (18–22 μmoles), except for experiment 6 in which bile amount was most likely overestimated (105 μmoles). The parameters obtained from experiment 6 were unexpectedly different from the 3 others (Fig. 4).

Validation of the Reduced Model With Radioactivity Data

As a validation exercise, the reduced model developed for MRI data was applied retrospectively to the radioactivity data of the liver, while ignoring bile and perfusate data. The model successfully described the liver data as indicated by the absence of any significant bias in the residuals (Fig. 3d). Estimated rate constants are summarized in Table 1. The precision of estimates was adequate, with standard errors $<$10% for all parameters. Between-experiment variability was low for all parameters. Standard deviations of the residual error were $<$0.1 μmoles and $<$0.6 μmoles when amounts in the liver were 0 and 11 μmoles, respectively.

Validation through parameters proceeded by comparison of estimates from the reduced and complete models. The reduced model provided similar rate constants as the complete model except for k_{12}(B) that was about 40% lower and k_{26}(B) that was about 15 times lower in the reduced model. The estimated rate constants were largely similar to those obtained from fitting the MRI data with the same reduced model (Table 1). The difference between the complete and reduced models was reflected by different kinetic profiles of compartments 2 and 6 (Fig. 3c and d). After 30-minute perfusion with Gd-BOPTA, predicted amounts of contrast agent in the extracellular (compartment 1) and cellular (compartments 2 + 6) spaces were similar in the 2 models (13% and 87% respectively). However, the distribution between compartments 2 and 6 changed, from 31% and 56% respectively in the complete model, to 77% and 10% in the reduced model.

Validation through predictions considered predicted amounts of contrast agent in bile and perfusate with respect to experimental data from radioactivity experiments. The model allowed good prediction of Gd-BOPTA amount in bile and perfusate (Fig. 3d). Gd-BOPTA amount in bile was slightly overestimated (mean prediction error for the 3 preparations: $-$1.8 μmoles) whereas Gd-BOPTA amount in perfusate was slightly underestimated (mean prediction error for the 3 preparations: +1.7 μmoles). These prediction errors were nevertheless small relative to total amount ($<$17% and 0.4% for bile and perfusate, respectively).

DISCUSSION

Qualitative differences in the behaviors of Gd-DTPA and Gd-BOPTA in the rat liver were observed with both radioactivity detection and MRI. The radioactivity and the signal intensity in the liver rapidly increased toward steady-state during perfusion of Gd-DTPA and returned to baseline during perfusion with KHB, showing extracellular distribution and subsequent complete elimination of the contrast agent. In contrast, the amount of contrast agent and the signal intensity continuously increased during the 30-minute perfusion of Gd-BOPTA indicating that, in addition to its extracellular distribution, Gd-BOPTA entered into hepatocytes. Its hepatic elimination was slow and incomplete over the observed washing period. Radioactivity experiments showed that no Gd-DTPA was extracted by the liver, in contrast to Gd-BOPTA that had a 5% extraction. The difference with the 50% excretion observed in vivo[6,12] is due to the absence of recirculation in the single-pass perfused livers as performed here.

We developed a pharmacokinetic model to analyze MR signal intensity as a function of time and quantify Gd-BOPTA transport in the liver, through physiologically relevant parameters reflecting bile excretion and potential bidirectional transport through transporters of the sinusoidal membrane. We first modeled together extracellular and hepatobiliary contrast agents and analyzed MR signal intensity as well as radioactivity measurements that included bile and perfusate amounts not available with MRI. Then, because model parameters are to be unambiguously and precisely estimated, a reduced form of the model was used for the MR signal, the performance of which was being investigated with respect to the complete model. A third aspect was the consideration of the relationship between the MR signal intensity and the contrast agent amounts. Signal in a region of interest was modeled as a sum of contributions from extracellular and hepatocyte-associated compartments, while taking into account background signal and possible signal saturation with increasing amounts of contrast agent in the liver.

A 6-compartment model with 8 rate constants was the simplest model that successfully described radioactivity data. Low standard errors of parameter estimates indicated that the model was fully identified from the experimental data. For Gd-DTPA the best fit was obtained with unidirectional exchange from the extracellular compartment toward a compartment postulated to reflect liver cells. However, the corresponding rate constant was more than 100 times lower than for Gd-BOPTA, suggesting a low level of cell trapping or tissue binding. A similar low trapping level was observed with isolated hepatocytes in suspension[31] and in a hollow-fiber bioreactor.[28] In contrast, a high amount of Gd-BOPTA distributed into hepatocytes with reverse transfer supposed to reflect Gd-BOPTA efflux through the sinusoidal membrane back to the perfusate, consistent with a bidirectional transport through Oatps[32,33] or with the efflux of Gd-BOPTA through Mrp3 or Mrp4[34] since Gd-BOPTA is a Mrp substrate.[11,12] From a first intracellular compartment (compartment 2), Gd-BOPTA was excreted into bile and transferred to a secondary hepatocyte-associated compartment (compartment 6). No reverse transfer was observed during the time course of the experiment. The fit significantly improved with the addition of this compartment. Although the perfusion of Gd-DTPA before Gd-BOPTA allows discrimination of the extracellular and intracellular volumes of the liver, the biologic relevance of the secondary cellular compartment is more difficult to interpret. Compartment 6 may only be mathematically distinct from compartment 2 or may have biologic relevance, eg, reflecting Gd-BOPTA trapping inside hepatocytes or Gd-BOPTA presence in bile canaliculi or both phenomena. Intracellular trapping could be explained by Gd-BOPTA binding to intracellular structures or by Gd-BOPTA changes in conformation in some specific cellular space that delay Gd-BOPTA biliary excretion. The biologic relevance of this compartment 6 will be improved by the use of the pharmacokinetic model in different experimental conditions, such as competition/inhibition studies. Nevertheless, such an additional cell-associated compartment has been described in the literature regarding pharmacokinetic modeling in the isolated perfused rat liver. Geng et al[35] described an additional "deep pool" within the hepatocyte reflecting the fact that bromosulfophthalein-glutathione distributed in 2 separate spaces in the hepatocyte. Proost et al[36] raised different hypotheses for an additional "liver storage" compartment of dibromosulfophtalein, such as binding to cytosolic proteins, uptake into mitochondria or transport vesicles.

In the absence of perfusate and bile data, a reduced number of rate constants were identifiable from MR signal intensity of the liver, leading to a reduced form of the model. However, estimated rate constants were largely similar to the ones obtained from the complete model and radioactivity data. The amount of Gd-BOPTA remaining after the washing period was similarly localized in the "trapping" compartment. Predictions of contrast agent amounts in perfusate and bile were consistent with the radioactivity experiments. For validation, the performance of the reduced model was tested with the radioactivity data of the liver, ignoring bile and perfusate data. The reduced model successfully fitted the radioactivity data of the liver, it provided largely similar parameter estimates as the complete model and allowed prediction of contrast agent amounts in perfusate and bile (prediction errors $<20\%$). Nevertheless, there was a larger interexperiment variability of raw data (Fig. 4) and pharmacokinetic parameters with MR than with radioactivity. This poor reproducibility of MRI data has already been identified as a real difficulty when performing pharmacokinetic modeling.[37–39]

Converting signal intensity to contrast agent amount or concentration is not obvious and has been explored by numerous groups.[22,24,25] For instance, Gd-DTPA and Gd-BOPTA have similar relaxivities in protein-free buffer, but Gd-BOPTA has a higher relaxivity in protein-containing solutions than Gd-DTPA.[40,41] Hence, the relaxivity in the liver extracellular fluid, and in the hepatocyte spaces may be different. In the present study however, a single proportionality constant relating signal intensity to contrast agent amount in liver compartments was compatible with mean signal intensity in a region of interest, as previously described.[28] Thus, MRI may not be able to define the inner

compartment of the liver. In addition, parallel analysis of MRI and radioactivity data supported a signal saturation at high contrast agent concentration rather than a saturation of Gd-BOPTA transport, the radioactivity data being compatible with linear processes. We used a FAST sequence because it has a high signal intensity sensitivity for the low contrast agent concentrations used in this study.[42,43] However, with this sequence, the range of contrast agent amount along which the signal intensity linearly increases is short and signal intensity rapidly saturates. This is the reason why an equation of saturation was integrated in the model.

In conclusion, we developed a compartmental pharmacokinetic model that successfully described the MR signal intensity recorded over time during perfusion of Gd-BOPTA and quantified the transport of Gd-BOPTA in rat liver. Perfusion of Gd-DTPA prior to Gd-BOPTA allowed distinction of the extracellular and intracellular components. By analyzing similar experiments performed with radiolabeled contrast agents and radioactivity measurements in liver, bile and perfusate we strengthen the physiological relevance of the pharmacokinetic model and provide quantification of Gd-BOPTA uptake and prediction of biliary excretion. The proposed model is also expected to provide useful information on the modification of the overall Gd-BOPTA transport that can occur in pathologic conditions.

REFERENCES

1. Hamm B, Kirchin M, Pirovano G, et al. Cinical utility and safety of Multihance in magnetic resonance imaging of liver cancer: results of multicenter studies in Europe an the USA. *J Comput Assist Tomogr*. 1999;23:S53–S60.
2. Manfredi R, Maresca G, Baron RL, et al. Gadobenate dimeglumine (BOPTA) enhanced MR imaging: patterns of enhancement in normal liver and cirrhosis. *J Magn Reson Imag.* 1998;862–867.
3. Schneider G, Maas R, Schultze Kool L, et al. Low-dose gadobenate dimeglumine versus standard dose gadopentetate dimeglumine for contrast-enhanced magnetic resonance imaging of the liver. *Invest Radiol*. 2003;38:85–94.
4. Kuwatsuru R, Kadoya M, Ohtomo K, et al. Comparison of gadobenate dimeglumine with gadopentetate dimeglumine for magnetic resonance imaging of liver tumors. *Invest Radiol*. 2001;36:632–641.
5. Schuhmann-Giampieri G, Frenzel T, Schmitt-Willich H. Pharmacokinetics in rats, dogs and monkeys of a gadolinium chelate used as a liver-specific contrast agent for magnetic resonance imaging. *Drug Res*. 1993;43:927–931.
6. Lorusso V, Arbughi T, Tirone P, et al. Pharmacokinetics and tissue distribution in animals of gadobenate ion, the magnetic resonance imaging contrast enhancing component of gadobenate dimeglumine 0.5 M solution for injection (MultiHance). *J Comput Assist Tomogr*. 1999;23:181–194.
7. Spinazzi A, Lorusso V, Pirovano G, et al. Multihance clinical pharmacology. *Acad Radiol*. 1998;5:86–89.
8. Clément O, Siauve N, Lewin M, et al. Contrast agents in magnetic resonance imaging of the liver: present and future. *Biomed Pharmacother*. 1998;52:51–58.
9. Hahn PF, Saini S. Liver-specific MR imaging contrast agents. *Radiol Clin North Am*. 1998;36:287–297.
10. Pastor CM, Planchamp C, Pochon S, et al. Kinetics of gadobenate dimeglumine in isolated perfused rat liver: MR imaging evaluation. *Radiology*. 2003;229:119–125.
11. Pascolo L, Petrovic S, Cupelli F, et al. ABC protein transport of MRI contrast agents in canalicular rat liver plasma vesicles and yeast vacuoles. *Biochem Biophys Res Commun*. 2001;282:60–66.
12. De Haën C, Lorusso V, Tirone P. Hepatic transport of gadobenate dimeglumine in TR$^-$ rats. *Acad Radiol*. 1996;3:452–454.
13. Vallée JP, Lazeyras F, Kasuboski L, et al. Quantification of myocardial perfusion with FAST sequence and Gd bolus in patients with normal cardiac function. *J Magn Reson Imag*. 1999;9:197–203.
14. Larsson HBV, Fritz-Hansen T, Rostrup E, et al. Myocardial perfusion modeling using MRI. *Magn Reson Med*. 1996;35:716–726.
15. Scharf J, Zapletal C, Hess T, et al. Assessment of hepatic perfusion in pigs by pharmacokinetic analysis of dynamic MR images. *J Magn Reson Imag*. 1999;9:568–572.
16. Materne R, Smith AM, Peeters F, et al. Assessment of hepatic perfusion parameters with dynamic MRI. *Magn Reson Med*. 2002;47:135–142.
17. Van Beers BE, Materne R, Annet L, et al. Capillarization of the sinusoids in liver fibrosis: noninvasive assessment with contrast-enhanced MRI in the rabbit. *Magn Reson Med*. 2003;49:692–699.
18. Peeters F, Annet L, Hermoye L, et al. Inflow correction of hepatic perfusion measurements using T1-weighted, fast gradient-echo, contrast-enhanced MRI. *Magn Reson Med*. 2004;51:710–717.
19. Tofts PS, Kermode AG. Measurement of the blood-brain barrier permeability and leakage space using dynamic MR imaging. 1. Fundamental concepts. *Magn Reson Med*. 1991;17:357–367.
20. Larsson HBV, Stubgaard M, Frederiksen JL, et al. Quantitation of blood-brain barrier defect by magnetic resonance imaging and gadolinium-DTPA in patients with multiple sclerosis and brain tumors. *Magn Reson Med*. 1990;16:117–131.
21. Roberts TP, Chuang N, Roberts HC. Neuroimaging: do we really need new contrast agents for MRI? *Eur J Radiol*. 2000;34:166–178.
22. Taylor JS, Reddick WE. Evolution from empirical dynamic contrast-enhanced magnetic resonance imaging to pharmacokinetic MRI. *Adv Drug Deliv Rev*. 2000;41:91–110.
23. Padhani AR. Dynamic contrast-enhanced MRI in clinical oncology: current status and future directions. *J Magn Reson Imaging*. 2002;16:407–422.
24. Evelhoch JL. Key factors in the aquisition of contrast kinetic data for oncology. *J Magn Reson Imaging* 1999;10:254–259.
25. Tofts PS. Modeling tracer kinetics in dynamic Gd-DTPA MR imaging. *J Magn Reson Imaging* 1997;7:91–101.
26. Tofts PS, Brix G, Buckley DL, et al. Estimating kinetic parameters from dynamic contrast-enhanced T1-weighted MRI of a diffusable tracer: standardized quantities and symbols. *J Magn Reson Imaging* 1999;10:223–232.
27. Planchamp C, Montet X, Frossard J-L, et al. Magnetic resonance imaging with hepatospecific contrast agents in cirrhotic livers. *Invest Radiol*. 2005;40:187–194.
28. Planchamp C, Gex-Fabry M, Dornier C, et al. Gd-BOPTA transport into rat hepatocytes: pharmacokinetic analysis of dynamic magnetic resonance images using a hollow-fiber bioreactor. *Invest Radiol*. 2004;39:506–515.
29. Pastor CM, Williams D, Yoneyama T, et al. Competition for tetrahydrobiopterin between phenylalanine hydroxylase and nitric oxide synthase in rat liver. *J Biol Chem*. 1996;271:24534–24538.
30. Port MD, Knopp MV, Hoffmann U, et al. Multicompartment analysis of gadolinium chelate kinetics: Blood-tissue exchange in mammary tumors as monitored by dynamic MR imaging. *J Magn Reson Imaging* 1999;10:233–241.
31. Thorstensen K, Romslo I. The interaction of gadolinium complexes with isolated rat hepatocytes. *BioMetals*. 1995;8:65–69.
32. Shi X, Bai S, Ford AC, et al. Stable inducible expression of a functional rat liver organic anion transport protein in HeLa cells. *J Biol Chem*. 1995;270:25591–25595.
33. Li L, Meier PJ, Ballatori N. Oatp2 mediates bidirectional organic solute transport: a role for intracellular glutathione. *Mol Pharmacol*. 2000;58:335–340.
34. Kullak-Ublick GA, Stieger B, Meier PJ. Enterohepatic bile salt transporters in normal physiology and liver disease. *Gastroenterology*. 2004;126:322–342.
35. Geng W, Schwab AJ, Horie T, et al. Hepatic uptake of bromosulfophthalein-glutathione in perfused Eisai hyperbilirubinemic mutant rat liver: a multiple-indicator dilution study. *J Pharmacol Exp Ther*. 1998;284:480–492.
36. Proost JH, Nijssen HMJ, Strating CB, et al. Pharmacokinetic modeling of the sinusoidal efflux of anionic ligands from the isolated perfused rat liver: the influence of albumin. *J Pharmacokin Biopharm*. 1993;21:375–394.

37. Galbraith SM, Lodge MA, Taylor NJ, et al. Reproducibility of dynamic contrast-enhanced MRI in human muscle and tumors: comparison of quantitative and semi-quantitative analysis. *NMR Biomed*. 2002;15:137–142.
38. van Laarhoven HWM, Rijpkema M, Punt CJA, et al. Methods for quantification of dynamic MRI contrast agent uptake in colorectal liver metastases. *J Magn Reson Imaging* 2003;18:315–320.
39. Jackson A, Haroon H, Zhu XP, et al. Breath-hold perfusion and permeability mapping of hepatic malignancies using magnetic resonance imaging and a first-pass leakage profile model. *NMR Biomed.* 2002;15:164–173.
40. Cavagna FM, Maggioni F, Castelli PM. Gadolinium chelates with weak binding to serum proteins. A new class of high-efficiency, general purpose contrast agents for magnetic resonance imaging. *Invest Radiol*. 1997;32:780–796.
41. De Haën C, Cabrini M, Akhnana L, et al. Gadobenate dimeglumine 0.5M solution for injection (Multihance): pharmaceutical formulation and physicochemical properties of a new magnetic resonance imaging contrast medium. *J Comput Assist Tomogr*. 1999;23:S161–S168.
42. Ivancevic MK, Zimine Y, Lazeyras F, et al. FAST sequences optimization for contrast media pharmacokinetic quantification in tissue. *J Magn Reson Imaging* 2001;14:771–778.
43. Vallée JP, Ivancevic MK, Lazeyras F, et al. Use of high flip angle in T1-prepared FAST sequences for myocardial perfusion quantification. *Eur Radiol*. 2003;13:507–514.